MITSUBISHI ELECTRIC RESEARCH LABORATORIES
https://www.merl.com

Magnetic Cooling with Thin Peltier Modules as Thermal Switches

Lin, Chungwei

TR2023-006 March 01, 2023

Abstract

Magnetic refrigeration is a promising alternative to the existing vapor-compression technology. The refrigerant of magnetic cooling is the magnetocaloric material whose temperature is controlled by applying/removing the magnetic field during the cooling cycle. In this work we consider the scenario where thin Peltier modules are used to control the heat flow in the magnetic cooling device. A phenomenological 3-parameter model is adopted to describe the Peltier modules, based on which we develop a simple numerical procedure to simulate the cooling device that includes both magnetocaloric materials and Peltier modules. Using coefficient of performance as the performance metric, we find that the inclusion of Peltier modules can greatly reduce the design complexity, particularly to simplify the pumping and valving systems of the working fluid. The same design concept can be applied to the cooling systems using solid refrigerants.

Journal of Magnetism and Magnetic Materials 2023

Mitsubishi Electric Research Laboratories, Inc.
201 Broadway, Cambridge, Massachusetts 02139

Magnetic Cooling with Thin Peltier Modules as Thermal Switches

Chungwei Lin
Mitsubishi Electric Research Laboratories, 201 Broadway, Cambridge, MA 02139, USA
(Dated: January 27, 2023)

Magnetic refrigeration is a promising alternative to the existing vapor-compression technology. The refrigerant of magnetic cooling is the magnetocaloric material whose temperature is controlled by applying/removing the magnetic field during the cooling cycle. In this work we consider the scenario where thin Peltier modules are used to control the heat flow in the magnetic cooling device. A phenomenological 3-parameter model is adopted to describe the Peltier modules, based on which we develop a simple numerical procedure to simulate the cooling device that includes both magnetocaloric materials and Peltier modules. Using coefficient of performance as the performance metric, we find that the inclusion of Peltier modules can greatly reduce the design complexity, particularly to simplify the pumping and valving systems of the working fluid. The same design concept can be applied to the cooling systems using solid refrigerants.

PACS numbers:

I. INTRODUCTION

Since the early demonstration [1] and the material breakthrough [2, 3], magnetic refrigeration is considered as one of the promising and environmentally friendly alternatives to the existing room-temperature vapor-compression technology [4–7]. The refrigerant of magnetic refrigeration is the magetocaloric material (MCM) whose temperature can be controlled by the applied magnetic field. During a cooling cycle, the refrigerant is cooled below the cold environment temperature so that it absorbs heat from the cold environment; it is then heated above the hot environment temperature so that it ejects heat to the hot environment. The primary reason that limits the usefulness of magnetic cooling is that MCM experiences a relatively small temperature change (about 5 K) in the reasonably accessible field strength (1-2 Tesla). From the implementation aspect, a typical MCM is a solid that cannot easily move between two spatially separate environments, so one needs to combine other mechanism to guide the heat flow. Two well-known solutions are the active magnetic regeneration (AMR) where a working fluid is introduced to move between two environments, and the cascading mechanism where thermal diodes are introduced to temporarily block the conductive heat flow between adjacent components (see Chapter 6 of Ref. [4]). Roughly, the AMR uses the thermal convection, i.e., the ordered motions of the fluid molecules, to produce the desired heat flow, whereas the cascading mechanism uses the thermal diodes/switches [8–10] to generate the temperature profile such that the thermal conduction gives the needed heat flow.

Peltier modules are a simple cooling device based on the thermoelectric effect [11, 12]. It is typically classified as a thermal switch because its function requires an energy input [13, 14]. Integrating Peltier modules in the magnetic cooling device is first proposed by Kitanovski and Egolf in [15], and more detailed simulations are presented subsequently in Ref. [4, 8, 9, 16–18]. There are two types of arrangement. For the AMR-based arrangement [8, 9, 16, 17], the working fluid is essential for transferring heat from the cold to the hot environment. Peltier modules are used to control the heat flow between MCM and working fluid; doing so reduces the complexity on the pumping/valving system. For the cascade arrangement [18], MCM's and Peltier modules are alternately placed in space and Peltier modules are the main components to generate heat flow against the environment. As a component, Peltier module can play the role of the working fluid that generates a desired heat flux, or the role of a thermal diode that blocks the conductive thermal flux, or something in between.

In this work we consider the cascade arrangement using *thin* Peltier modules as thermal switches. Peltier module is described by a phenomenological model where the *ordered* motions of charge carriers, which can be controlled by applied current, are responsible for the tunable heat flux. A numerical procedure to simulate the cooling devices is developed to include both MCM units and Peltier modules. Gadolinium (Gd), the "reference material" for room-temperature magnetic energy conversion [6, 19–21], is used as the MCM. We take the experimental specific heat and adiabatic temperature change [22] to ensure the consistency. As MCM is not the main cost in the cooling device (compared to the cost to generate the magnetic field), we use COP (Coefficient Of Performance) as the performance metric. In other words, one can place multiple MCM/Peltier units between reservoirs to increase cooling power. Generally, the conventional AMR setup gives better cooling performance because the MCM-to-fluid heat transfer can be made large by increasing the contact surface area and the energy loss by pumping the fluid is relatively small. For the cascade arrangement, our analysis indicates that the real advantage brought by Peltier modules is not about the performance enhancement but about the reduction of device complexity while maintaining a reasonable COP.

The paper is organized as follows. In Section II we summarize the minimal model of a Peltier module, verify the

model by comparing with products, and introduce the numerical procedure to simulate the system composed of Peltier modules and MCM units. From Section III to V we gradually introduce components to the overall cooling device in order to lessen the burden of Peltier modules and ultimately increase COP. In Section III we examine the performance of Peltier cooling alone which will be served as the reference. In Section IV we combine the Peltier modules with the magnetic cooling and show that only a modest enhancement in COP can be achieved. In Section V we further integrate the working fluid in the cooling device and show that a significant enhancement in COP can be achieved. General remarks based on the simulation results in Sections III-V are given. In particular, some qualitative behavior and an illustrative realization are presented. A brief conclusion and future direction will be provided in Section VI.

II. DESCRIPTIONS OF IMPORTANT COMPONENTS

In this section we provide the necessary information for the simulation, including the MCM properties, a simple model of the Peltier module. A numerical procedure is developed to simulate the spatial-temporal temperature distribution, and its limitation is pointed out.

A. Material properties of MCM

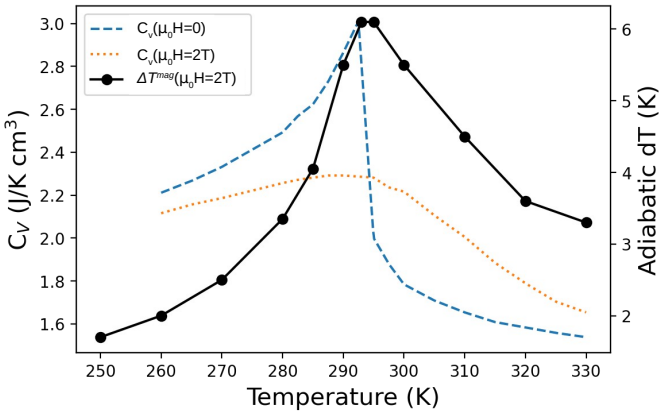

FIG. 1: Volume specific heat (left y-axis) and adibatic temperature change (right y-axis) for Gd between $\mu_0 H = 0$ and 2T. Data are taken from Ref. [22].

MCM is the heart of the magnetic cooling, and we use Gd as the MCM. Three material properties are needed to simulate the cooling cycle: the specific heat, the adiabatic temperature change (upon field change), and the thermal conductivity. The first two quantities have strong temperature and field dependence, whereas the last one is to a good approximation a constant over the temperature range of interest (room temperature).

We shall consider the cooling cycle operated at two fields $\mu_0 H = 0$ and $\mu_0 H = 2$T; this field choice is partly due to its convenient experimental availability. From Ref. [22], the volume specific heat at $\mu_0 H = 0$ and $\mu_0 H = 2$T are given in Fig. 1 (left y-axis). The adiabatic temperature change upon magnetizing MCM from zero field to a finite field of $\mu_0 H$ is denoted as $\Delta T^{\rm mag}(\mu_0 H, T)$ (>0); the adiabatic temperature change upon demagnetizing MCM from a finite field of H to zero field is denoted as $\Delta T^{\rm dem}(\mu_0 H, T)$ (<0). They are related by

$$\Delta T^{\rm mag}(\mu_0 H, T) = -\Delta T^{\rm dem}\big(\mu_0 H, T + \Delta T^{\rm mag}(\mu_0 H, T)\big). \tag{1}$$

$\Delta T^{\rm mag}(\mu_0 H, T)$ for $\mu_0 H = 2$T is provided in Fig. 1 (right y-axis); $\Delta T^{\rm mag}$ and the corresponding $\Delta T^{\rm dem}$ obtained from Eq. (1) will be used in the subsequent simulations. The thermal conductivity is assumed to be temperature and field independent: throughout this work we use $\kappa_{\rm Gd} = 0.088$ W/cm K. We note that the mean-field approximation gives a reasonable estimate of the adiabatic temperature change but not the specific heat [19, 21, 23]; taking the experimental data for both quantities ensures a more realistic and consistent description of the system [24].

B. Minimum model for Peltier modules

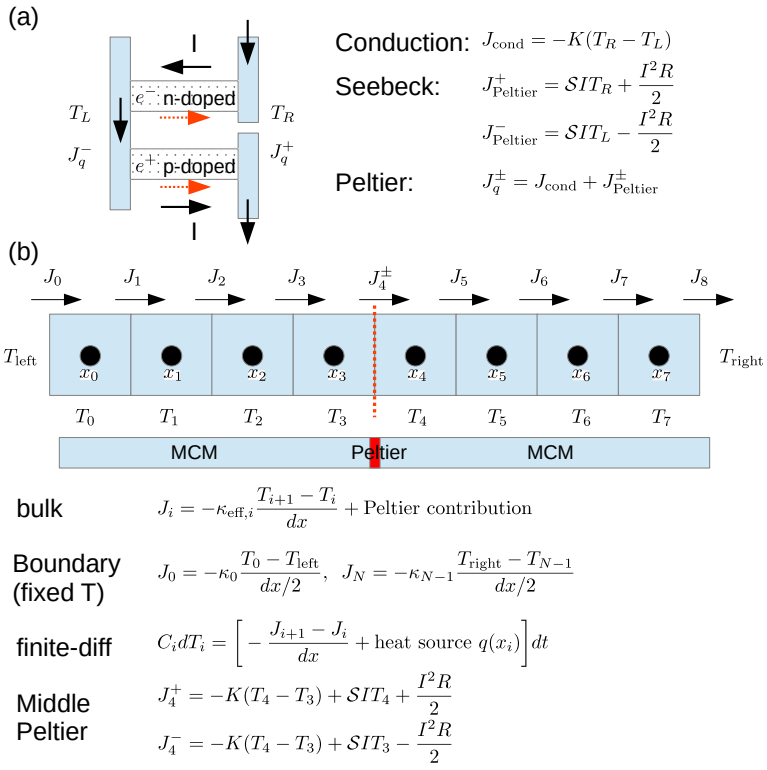

FIG. 2: (a) The heat flux within a Peltier module. For the applied current following the black arrows, both electrons in n-doped region and holes in p-doped move from left to right. The Peltier contribution is given by $\mathcal{S}IT$. The flux generated by Ohm loss I^2R equally flows to both sides. (b) Finite-difference scheme for diffusion equation. The nodes for temperature and those for flux are alternate in space. The red dotted line in the middle can represent a thin Peltier module which has a different thermal conductivity to the bulk (Gd) material. In our simulation, the Peltier module provides a discontinuity in the heat flux and its internal temperature distribution is not considered.

A good phenomenological description of thermoelectric or Peltier module has been established [11, 12]. As illustrated in Fig. 2(a), a Peltier module places electron-doped and hole-doped semiconductors (such as bismuth telluride, Bi_2Te_3 or silicon) between two heat reservoirs. When applying a current following black solid arrow, both electrons and holes as charge carriers move from the left side to the right side. This process brings the heat from the left to the right environment no matter the environment temperatures. The Peltier effect can be regarded as a convective process as it represents the externally-controlled ordered motion of charge carriers that contributes to the heat flux. The complete analogy to the convection by water flow is as follows: the water molecules $\leftrightarrow$ charge carriers; the pump driving the water flow $\leftrightarrow$ applied voltage or current; the viscous loss upon maintaining the water flow $\leftrightarrow$ Ohm loss.

We consider the thin Peltier module whose thickness is smaller than (the linear dimension of) its cross section. Quantitatively we use three parameters to specify a thin Peltier module of cross section A: (i) $\frac{\mathcal{S}}{A}$, which has the dimension V$\cdot$ K$^{-1}\cdot$cm^{-2}, is the thermoelectric power per area; (ii) $\frac{R}{A}$, which has the dimension Ohm$\cdot$cm^{-2}, is the resistance per area; (iii) $\frac{K}{A}$, which has the dimension W$\cdot$K$^{-1}\cdot$cm^{-2}, is the thermal conductance per area. In (i), $\mathcal{S} = n(S_{\text{p-doped}} - S_{\text{n-doped}}) = n(|S_{\text{p-doped}}| + |S_{\text{n-doped}}|)$ where S is the Seebeck coefficient of the material and n is the number of p-doped/n-doped semiconductor pair that connect two environments in the module. As an illustration, Fig. 2(a) corresponds to one connecting pair of p-doped/n-doped semiconductors. Note that all $\mathcal{S}$, R, K are proportional to the number of connecting pairs and thus the cross section. Applying the current I to a thin Peltier module that

connects the left/right environment of temperature $T_{\rm L}/T_{\rm R}$, the total heat fluxes at both sides are

$$J_{\rm L} = \mathcal{S}IT_{\rm L} - K\Delta T - \frac{1}{2}I^2R, \tag{2a}$$

$$J_{\rm R} = \mathcal{S}IT_{\rm R} - K\Delta T + \frac{1}{2}I^2R, \tag{2b}$$

with $\Delta T = T_{\rm R} - T_{\rm L}$. Dividing Eqs. (2) by the cross section gives the flux per area. In Eqs. (2), $\mathcal{S}IT$ is from the Peltier effect that resembles the convective contribution; $-K\Delta T$ is from the thermal conduction; I^2R is the Ohm loss which dissipates equally to both reservoirs. The input work and the corresponding COP are

$$W_{\rm Peltier} = I\big[\mathcal{S}\,\Delta T + IR\big], \tag{3a}$$

$$\mathrm{COP} = \frac{J_{\rm L}}{W_{\rm Peltier}} = \frac{\mathcal{S}IT_{\rm L} - K\Delta T - \frac{1}{2}I^2R}{\mathcal{S}I\Delta T + I^2R}. \tag{3b}$$

Both thermal conduction and electric resistance generate entropy and reduce COP; Carnot COP is achieved when $K = 0$ and $R = 0$.

Eqs. (2) can be used to compute the performance of a Peltier module. Two important limits are highlighted. First, for a given cold temperature $T_{\rm cold}$, the maximum temperature span is given by

$$\Delta T_{\rm max} = T_{\rm hot} - T_{\rm cold} = \frac{1}{2}\left[\frac{\mathcal{S}^2}{RK}\right]T_{\rm cold}^2 \equiv \frac{1}{2}\mathcal{Z}T_{\rm cold}^2. \tag{4}$$

Here $\mathcal{Z} \equiv \frac{\mathcal{S}^2}{RK}$ which has the dimension K^{-1}. The maximum temperature span corresponds to zero heat removal from the cold environment. Under the $\Delta T_{\rm max}$ condition, the applied voltage and resulting current are

$$V_{\Delta T_{\rm max}}(T_{\rm hot}, T_{\rm cold}) = \mathcal{S}T_{\rm hot}, \tag{5a}$$

$$I_{\Delta T_{\rm max}}(T_{\rm hot}, T_{\rm cold}) = \mathcal{S}T_{\rm cold}/R. \tag{5b}$$

Second, when both reservoirs have the same temperature T, the maximum heat flux is given by

$$J_{\rm max}(T) = \frac{1}{2}\frac{\mathcal{S}^2}{R}T^2 = \frac{1}{2}K\mathcal{Z}T^2. \tag{6}$$

For completeness, requiring maximum COP leads to

$$\begin{aligned} I_{\text{max-cop}} &= \frac{\mathcal{S}\Delta T}{R\left[\sqrt{1+\bar{\mathcal{Z}}T_M}-1\right]}, \\ \mathrm{COP}_{\rm max} &= \frac{T_{\rm cold}\left[\sqrt{1+\bar{\mathcal{Z}}T_M} - T_{\rm hot}/T_{\rm cold}\right]}{(T_{\rm hot}-T_{\rm cold})\left[\sqrt{1+\bar{\mathcal{Z}}T_M}+1\right]}. \end{aligned} \tag{7}$$

with $T_M = (T_{\rm hot} + T_{\rm cold})/2$ the average temperature.

Eqs. (4), (5), and (6) allow us to estimate K, R, $\mathcal{S}$ from the Spec sheets of real products. The results for two selected Peltier modules, roughly corresponding to two ends of electric resistivity, are given in Table I. For tens of products we have tested, Petier module of larger electric resistance has a larger Seebeck coefficient. Details of the fitting procedure and two self-consistency checks will be provided in Appendix. With $\frac{K}{A}$ one can also estimate the

module #	dimension (cm)	$\frac{\mathcal{S}}{A}$ $(\frac{\mathrm{V}}{\mathrm{K\,cm^2}})$	$\frac{R}{A}$ $(\frac{\mathrm{Ohm}}{\mathrm{cm^2}})$	$\frac{K}{A}$ $(\frac{\mathrm{W}}{\mathrm{K\,cm^2}})$	$\mathrm{COP}_{\rm max}$
(1) CP081030-M	1×1×0.3	0.02933	9.85	0.035	3.299
(2) CP200543636	5.4×3.6×0.36	0.00146	0.017	0.047	3.478

TABLE I: Parameters for two selected Peltier modules. Product information are provided in Appendix. Their performances under the operation condition $T_{\rm cold} = 280\mathrm{K}$, $T_{\rm hot} = 290\mathrm{K}$ are provided in Fig. 3(a), (b); the corresponding $\mathrm{COP}_{\rm max}$ evaluated from Eq. (7) are given in the last column.

thermal conductivity of the material used in Peltier module:

$$\kappa_{\rm Peltier} \approx \frac{K}{A} \times \text{thickness} \approx 0.01 - 0.02\ \mathrm{W/(cm\ K)}, \tag{8}$$

The Peltier material used in the product is Bi_2Te_3 whose thermal conductivity is about 0.01-0.03 W/(cm K) [26, 27], in reasonable agreement with the conductance (K) estimation.

Eqs. (2) are the steady-state results. In the following calculations we shall assume Eqs. (2) is reached instantaneously upon changing boundary temperatures during a cooling cycle. For this reason we estimate the time scale to reach the steady-state distribution within the Peltier module. It can be estimated from the heat diffusion equation $\frac{\partial T}{\partial t} = \alpha \frac{\partial^2 T}{\partial x^2}$, where $\alpha = \frac{\kappa}{\rho_s c_p}$ is the thermal diffusivity. Given L the size of the 1D problem, the solution corresponding to the vanishing boundary values and the slowest damping mode is $T(x,t) = e^{-t/\tau} \sin \frac{\pi x}{L}$ with the time constant $\tau = \frac{(L/\pi)^2}{\alpha}$; τ is identified as the relaxation time to reach the steady-state distribution. For Bi_2Te_3, $\kappa \approx 2.11$ W/m K, $\rho_s \approx 7600$ kg/m^3 and $c_p \approx 165$ J/Kg K [27] lead to $\alpha = 1.68$ mm^2/sec. For $L = 3$mm/4mm, the time constant is about 0.54/0.96 sec. To use the steady-state result Eqs. (2), the half period has to be longer than the relaxation time. We choose the minimum period to be 1 sec. From this respect, using the Silicon-based Peltier modules can be advantageous due to its short relaxation time [25].

C. Peltier module as a *continuous* thermal switch

As an active device the Peltier module can play different roles as a thermal component. Let us explicitly state its function and the corresponding terminology using Eqs. (2). Assuming $\Delta T > 0$, there is a natural (conductive) heat flux from right to the left (along -x direction) due to the environment. By varying I in Eq. (2a), we can have (i) $J_L > 0$ where the Peltier module acts as a *cooling* device; (ii) $J_L = 0$ where the Peltier module as a thermal *diode*; (iii) $J_L < 0$ where the Peltier module enhances the natural heat flux. Regarding I as a control parameter, all these functions will be explored in this work. We use the term "continuous thermal switch" to emphasize its ability to control the heat flow in either direction.

Quantitatively from Eqs. (2), the current required to block the conductive heat from the right reservoir of $T_{\rm R}$ to the left one of $T_{\rm L}$ (again $\Delta T \equiv T_{\rm R} - T_{\rm L} > 0$) is obtained by $J_{\rm L}(I_{\rm b}) = 0$:

$$\begin{aligned} I_b &= \frac{1}{R}\left[\mathcal{S}T_{\rm L} - \sqrt{(\mathcal{S}T_{\rm L})^2 - 2RK\cdot\Delta T}\right] \\ &\xrightarrow[R\to 0]{} \frac{K\cdot\Delta T}{\mathcal{S}T_{\rm L}} + \frac{R(K\cdot\Delta T)^2}{2(\mathcal{S}T_{\rm L})^3}. \end{aligned} \tag{9}$$

The small R (or large $\mathcal{S}$) expression explicitly shows the heat flux induced by the applied current compensates that from heat conduction. We bear in mind that $J_{\rm R}(I_b) = \mathcal{S} I_b \Delta T + I_b^2 R$ is always positive; blocking the heat flux has to come with Ohm loss. We can also enhance the heat flux from $T_{\rm R}$ to $T_{\rm L}$ by applying the current such that the charge carriers moving from right to left; enhancing the heat flux also comes with Ohm loss. In the configurations considered in this work, Peltier module is the only component that can generate heat flux against the environment.

D. Thin Peltier module between MCM units

We now describe how to simulate the temperature evolution including the Peltier module. The minimal setup is provided in Fig. 2(b) where a Peltier module is sandwiched by two MCM units; the temperature in each MCM unit satisfies the 1D heat diffusion equation:

$$C_v(T(x,t), h(x,t)) \frac{{\rm d}T(x,t)}{{\rm d}t} = -\frac{\rm d}{{\rm d}x} J(x) + q(x) \tag{10}$$

Here C_v is the volume specific heat which depends on the field $h(x)$ and the temperature $T(x)$, $J(x)$ is the heat flux density, and $q(x)$ is the heat source per volume. A useful numerical scheme is to store the flux J and temperature T at "staggered" grid points [28, 29]:

$$\begin{cases} T_i = T(x_i) & x_i = (i+\frac{1}{2}){\rm d}x \text{ where } i = 0, 1, \cdots, N-1 \\ J_i = J(\bar{x}_i) & \bar{x}_i = i\cdot {\rm d}x \text{ where } i = 0, 1, \cdots, N \end{cases} \tag{11}$$

The system is discretized into N equally-sized cells; each cell is of ${\rm d}x$ long. The heat source $q(x_i)$ resides on the same points of $T(x_i)$. The finite-difference equation is then

$$C_v(T_i, h_i){\rm d}T_i = \left[-\frac{J_{i+1} - J_i}{{\rm d}x} + q(x_i)\right]{\rm d}t \tag{12}$$

If the boundary condition is specified by the flux at two end points (i.e., Neumann boundary condition), we fix $J(x_0)$ and $J(x_N)$. If the temperatures at two end points are fixed (i.e., Dirichlet boundary condition) and the heat flux is governed by the heat conduction, then the flux at two boundary ends are

$$\begin{aligned} J(x_0) &= -\kappa(0)\frac{T(x_i) - T_{\text{left}}}{\mathrm{d}x/2}, \\ J(x_N) &= -\kappa(L)\frac{T_{\text{right}} - T(x_{N-1})}{\mathrm{d}x/2}, \end{aligned} \tag{13}$$

with κ the thermal conductivity. An example of $N = 8$ is shown in Fig. 2(b).

Applying the current I to a Peltier module has two effects: a convective contribution to the flux $\sim \mathcal{S}IT$ and a Ohm loss term I^2R. When placing a thin Peltier module at $L_0 = m \cdot \mathrm{d}x$, i.e., between two temperature points x_{m-1} and x_m, Eqs. (2) yields

$$\begin{aligned} J_m^- &= \mathcal{S}IT_{m-1} - K(T_m - T_{m-1}) - \frac{I^2R}{2}, \\ J_m^+ &= \mathcal{S}IT_m - K(T_m - T_{m-1}) + \frac{I^2R}{2}. \end{aligned} \tag{14}$$

Eq. (14) is illustrated in Fig. 2(a). Using this approximation, the transient behavior within the Peltier module is totally neglected and the effects of Peltier module are completely encoded in a discontinuity in heat flux without additional discritization points.

III. REFERENCE PROBLEM: PELTIER COOLING

In this section we consider the cooling performance involving *only* Peltier modules. The environment temperatures are fixed at $T_{\text{hot}} = 290\text{K}$, $T_{\text{cold}} = 280\text{K}$ which will be used for configurations including MCM's. The cooling powers and COP's for two modules in Table I are shown in Fig. 3(a) and (b). It is seen that the 2nd module has a better overall performance. We shall use the 1st module in the magnetic cooling system to illustrate that typical Peltier modules are adequate for tasks required in the magnetic cooling system.

A. Constant intermediate temperatures

To have a closer analogy to the multi-stage cooling, we consider the cooling using multiple Peltier modules between T_{hot} and T_{cold} with n intermediate temperatures; this requires $n+1$ Peltier modules which are labeled from 0 to n as shown in Fig. 3(c). The heat flux across the ith Peltier module experiences a current-dependent discontinuity; they are denoted as $J_i^{\pm}$ [same notation as Eq. (14)]. Maintaining *constant* intermediate temperatures requires $J_i^+ = J_{i-1}^-$, and the overall COP is given by $\frac{J_0^-}{J_n^+ - J_0^-}$. We find that the maximum COP happens when the intermediate temperatures are (nearly) equally-spaced between T_{hot} and T_{cold}, i.e.,

$$T_i = T_{\text{cold}} + i\frac{T_{\text{hot}} - T_{\text{cold}}}{n+1}. \tag{15}$$

The COP's as a function of input current of the 0th are provided in Fig. 3(d). We see that the maximum COP depends very weakly on the number of intermediate temperatures; the corresponding current and cooling power both decrease as n increases. Fig. 3(e) and (f) compare the COP's for different intermediate temperatures; it is seen that T_i's that obey Eq.(15) result in the largest COP. The resulting maximum COP depends very weakly on the number of intermediate temperatures, although $\text{COP}_{\max}$ does increase about $\lesssim 1\%$ as n increases.

B. Alternating intermediate temperatures

As will be seen in following sections, when combining with magnetic cooling the intermediate temperatures between Peltier modules are not constant in time. To mimic these situations we consider intermediate temperatures that alternate between two values: at stage one the intermediate temperature is $T_i^{(1)}$; at stage two $T_i^{(2)}$. For one intermediate

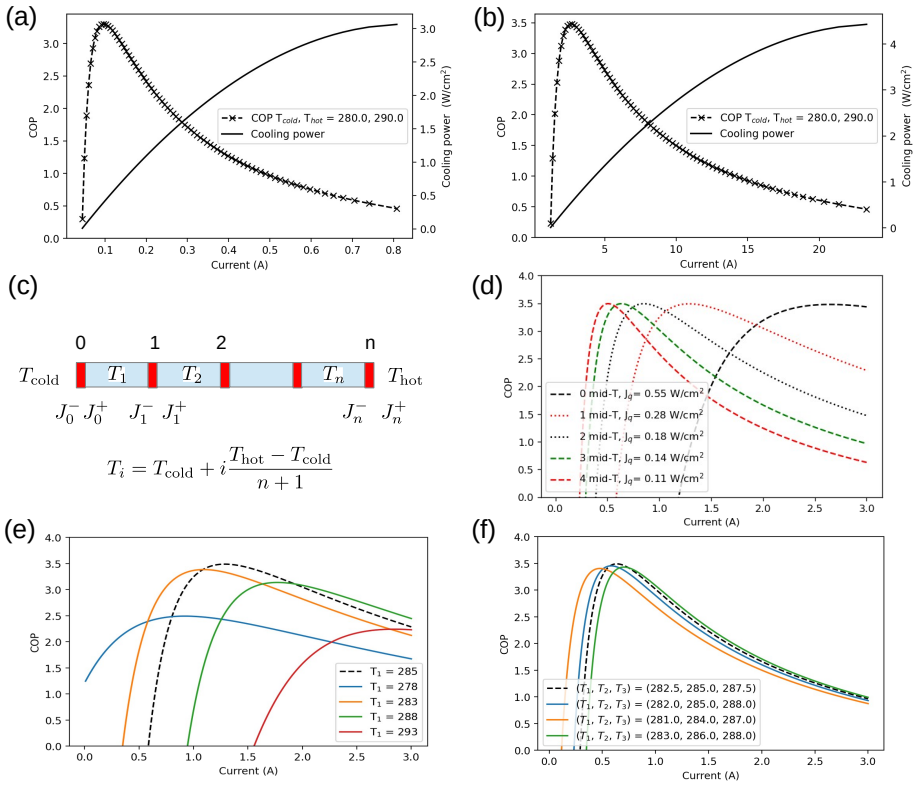

FIG. 3: The Peltier performance under the operation condition $T_{\rm cold} = 280$K, $T_{\rm hot} = 290$K. (a), (b) are respectively for modules (1), (2) in Table I. COPs for two modules are close: the maximum COP for (a) is 3.30, that for (b) is 3.48 [see Table I]. Device (2) has a larger cooling power. (c) The configuration including n equally-spaced intermediate temperatures. The red rectangles represent the Peltier modules, labeled from 0 to n; across ith Peltier module the heat flux experiences a discontinuity denoted as $J_i^{\pm}$ (i=0 to n). (d) The overall COPs for configuration (c) with the Peltier module characterized by (b). The maximum COPs are roughly a constant; the corresponding cooling power decreases. (e) Results from one intermediate temperature. (f) Results from three intermediate temperatures. In (e) and (f), having equally-spaced intermediate temperatures (dashed black curves) results in the largest COP.

temperature, the currents applied to two Peltier modules are $I_0^{(1)}$, $I_1^{(1)}$ at stage one; $I_0^{(2)}$, $I_1^{(2)}$ at stage two. At stage one, the flux across each Peltier module is given by

$$\begin{aligned}
J_0^{-,(1)} &= -K(T_1^{(1)} - T_{\rm cold}) + \mathcal{S} I_0^{(1)} T_{\rm cold} - \left(I_0^{(1)}\right)^2 R/2, \\
J_0^{+,(1)} &= -K(T_1^{(1)} - T_{\rm cold}) + \mathcal{S} I_0^{(1)} T_1^{(1)} + \left(I_0^{(1)}\right)^2 R/2, \\
J_1^{-,(1)} &= -K(T_{\rm hot} - T_1^{(1)}) + \mathcal{S} I_1^{(1)} T_1^{(1)} - \left(I_1^{(1)}\right)^2 R/2, \\
J_1^{+,(1)} &= -K(T_{\rm hot} - T_1^{(1)}) + \mathcal{S} I_1^{(1)} T_{\rm hot} + \left(I_1^{(1)}\right)^2 R/2.
\end{aligned} \tag{16}$$

At stage two, $J_0^{\pm,(2)}$, $J_1^{\pm,(2)}$ are obtained by replacing $T_1^{(1)}$ by $T_1^{(2)}$, $I_{0,1}^{(1)}$ by $I_{0,1}^{(2)}$. Imposing zero net flux into each intermediate region, i.e.,

$$J_i^{+,(1)} - J_{i+1}^{-,(1)} + J_i^{+,(2)} - J_{i+1}^{-,(2)} = 0, \tag{17}$$

ensures that no heat accumulates in the intermediate regions over a complete cycle so the process can be repeated as long as one would like to. Eq. (17) gives one constraint on the applied currents: given $(I_0^{(1)}, I_1^{(1)}, I_0^{(2)})$, $I_1^{(2)}$ is fixed. The overall COP after two stages is given by

$${\rm COP}_{\text{1-int, 2-stage}} = \frac{J_0^{-,(1)} + J_0^{-,(2)}}{\left(J_1^{+,(1)} + J_1^{+,(2)}\right) - \left(J_0^{-,(1)} + J_0^{-,(2)}\right)}. \tag{18}$$

We have done exhaustive parameter scans. During the scan, we first select an $I_1^{(0)}$ and do a 2D scan over $I_1^{(1)}$ and $I_0^{(2)}$ [$I_1^{(2)}$ is determined by Eq. (17)]. We find that COP is larger when the condition $|T_1^{(1)} - T_{\rm cold}| \approx |T_1^{(2)} - T_{\rm hot}|$ is

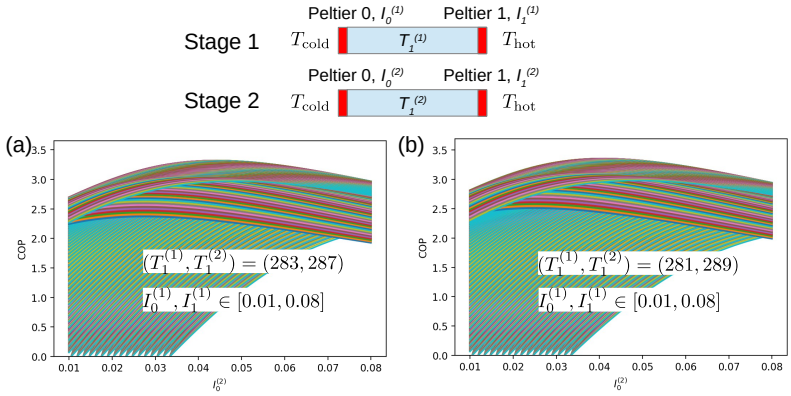

FIG. 4: Results of alternating one intermediate temperature. The schematic is shown on the top. (a) The intermediate temperature are alternating between $(T_1^{(1)}, T_1^{(2)}) = (283, 287)$. The maximum COP is around 3.32, occurred at $(I_0^{(1)}, I_1^{(1)}, I_0^{(2)}, I_1^{(2)}) = (0.05, 0.047, 0.044, 0.053)$. (b) $(T_1^{(1)}, T_1^{(2)}) = (281, 289)$. The maximum COP is around 3.35, occurred at $(I_0^{(1)}, I_1^{(1)}, I_0^{(2)}, I_1^{(2)}) = (0.051, 0.043, 0.041, 0.055)$.

approximately satisfied. Results for $(T_1^{(1)}, T_1^{(2)}) = (283, 287)$, $(T_1^{(1)}, T_1^{(2)}) = (281, 289)$ are shown in Fig. 4(a) and (b); the maximum COP of the former is 3.32 whereas that of the latter 3.35. The maximum $\mathrm{COP}_{\text{2-stage}}$'s can be slightly larger than, but are still very close to the maximum COP using a single Peltier module ($\sim$3.3). We also consider two intermediate temperatures where the search space includes four (2 stages and 2 regions) temperatures and six (2 stages and 3 Peltier modules) Peltier currents, with two constraints from Eq. (17). Using some random search the best COP value we found is still around 3.3. Notice that, because the heat loss other than those from Peltier modules (for example due to thermal conduction or transient behavior within the intermediate regions) is neglected in this analysis, the real COP can be only smaller than the estimated values.

As a brief summary, introducing piece-wise constant intermediate temperatures does not enhance COP in any meaningful way (about 1-2 % in the ideal situation). Although the intermediate temperatures allow a Peltier module to operate at a smaller temperature difference which results in a smaller Ohm loss, the corresponding heat removal rate is also reduced; the net effect on COP turns out to be insignificantly small.

IV. MAGNETIC COOLING CYCLE WITH PELTIER MODULES

Now we integrate the Peltier modules in the magnetic cooling setup and address the following question: how the combination of Peltier module and magnetic cooling improve the cooling performance compared to that of the Peltier cooling alone? The reference is a single Peltier module connecting two reservoirs of temperatures $T_{\rm left}$ and $T_{\rm right}$ [see Fig. 3(a), (b)]. What does the magnetic cooling bring? As MCM temperatures are controlled by the magnetic field, the Peltier modules do not account for all the cooling so they can work under a condition (i.e., smaller temperature difference) of higher efficiency [4, 8, 9]. Practically MCM also provide the intermediate temperatures as discussed in the previous section, and the key difference is that the zero net flux over a cooling cycle Eq. (17) has to include the contribution from the magnetocaloric effect.

A. Problem setup

The configurations considered are illustrated in Fig. 5(a), where n MCM units and two environments are separated by $n+1$ Peltier modules. The temperature distribution is determined by the 1D heat diffusion equation:

$$\begin{aligned} C_v(\mu_0 H(x,t), T(x,t))\frac{\mathrm{d}T(x,t)}{\mathrm{d}t} &= -\frac{\mathrm{d}}{\mathrm{d}x}J(x,t) + q_{\rm field}(x,t) + q_{\rm env}(x,t) \\ J(x) &= -\kappa_{\rm Gd}\frac{\mathrm{d}}{\mathrm{d}x}T(x,t) + \text{Peltier boundary condition} \end{aligned} \tag{19}$$

Eq. (19) is the same as Eq. (10) with explicit expressions on the heat sources and boundary conditions. $q_{\rm env}$ represents the heat exchange between the environment and the MCM, and its explicit form will be specified in Section V A;

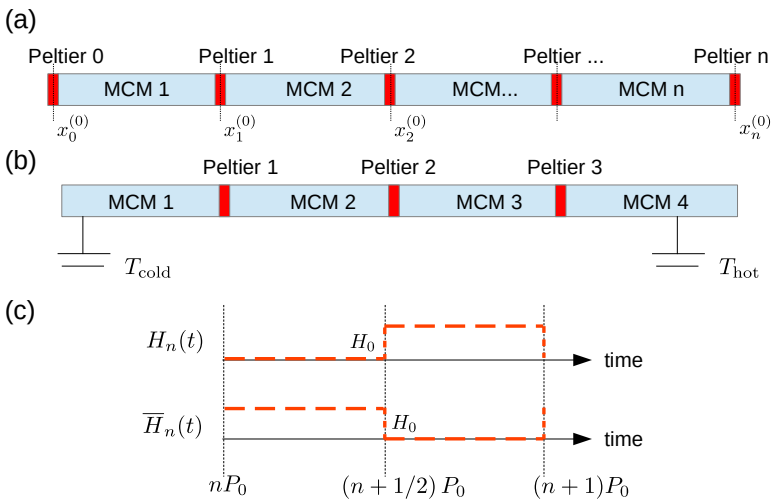

FIG. 5: (a) The configuration where $n+1$ Peltier modules are placed between n MCM units and between MCM unit and the environment. In this case the heat exchange is channeled through the two Peltier modules adjacent to the environments. With our simulation scheme, ith Peltier module is placed at $x_i^{(0)}$ with zero thickness; the applied current induces a discontinuity in heat flux across $x_i^{(0)}$ such that $J(x_i^{(0),+}) \neq J(x_i^{(0),-})$. (b) The configuration where $n-1$ Peltier modules are placed between n MCM units and between MCM unit and the environment. Leftmost and rightmost MCM units directly exchange heat with cold and hot environments respectively. (c) Two possible field as a function of time over a cycling period P_0.

in this section $q_{\rm env} = 0$. The following approximations are made to simplify the calculation. (i) The field change is assumed to be instantaneous between $\mu_0 H_0 = 0$T and $\mu_0 H_0 = 2$T, i.e., $H(x,t)$ is either 0 or H_0. For the cycling period of P_0, the field at each x as a function of time is either $H_n(t)$ or $\overline{H}_n(t)$:

$$\begin{aligned} H_n(t) &= H_0\Big[\Theta\big(t-(n+1/2)P_0\big) - \Theta\big(t-(n+1)P_0\big)\Big], \\ \overline{H}_n(t) &= H_0\Big[\Theta\big(t-nP_0\big) - \Theta\big(t-(n+1/2)P_0\big)\Big], \end{aligned} \tag{20}$$

for $nP_0 < t < (n+1)P_0$. Eqs. (20) are illustrated in Fig. 5(b). With instantaneous field change, Eq. (19) needs only $C_v(\mu_0 H, T)$ at $\mu_0 H = 2$T and 0 which are provided in Fig. 1. (ii) Following (i), the heat source upon field change is given by

$$q_{\rm field}(x,t) = C_v(\mu_0 H(x,t), T(x,t))\frac{\rm d}{{\rm d}t}\Delta T^{\rm ad}(T(x,t)) \tag{21}$$

$\Delta T^{\rm ad}$ can be $\Delta T^{\rm mag}(\mu_0 H, T)$ or $\Delta T^{\rm dem}(\mu_0 H, T)$ where $\mu_0 H = 2$T. Consider a point in Fig. 5(a) experiencing a field $H_n(t)$, from $t = (n+1/2)P_0 - \varepsilon$ to $t = (n+1/2)P_0 + \varepsilon$ a sudden temperature jump $\Delta T^{\rm mag}(\mu_0 H_0, T)$ occurs; from $t = (n+1)P_0 - \varepsilon$ to $t = (n+1)P_0 + \varepsilon$ a sudden temperature drop $-\Delta T^{\rm dem}(\mu_0 H_0, T)$ occurs. (iii) As shown in Fig. 5(a), the Peltier modules are placed at $x_i^{(0)}$ with $i = 0$ to n, and $J(x)$ is piece-wise continuous. For the domain $x \in (x_i^{(0)}, x_{i+1}^{(0)})$, the Peltier modules impose the boundary conditions on the heat flux:

$$\begin{aligned} J(x_i^{(0),+}) &= -K\big[T(x_i^{(0),+}) - T(x_i^{(0),-})\big] + \mathcal{S} I_i T(x_i^{(0),+}) - \frac{1}{2} I_i^2 R, \\ J(x_{i+1}^{(0),-}) &= -K\big[T(x_{i+1}^{(0),+}) - T(x_{i+1}^{(0),-})\big] + \mathcal{S} I_{i+1} T(x_{i+1}^{(0),-}) - \frac{1}{2} I_{i+1}^2 R \end{aligned} \tag{22}$$

where I_i is the current applied to ith Peltier module. (iv) The boundaries at two ends are fixed at $T_{\rm left} = 280$K and $T_{\rm right} = 290$K.

The steady-state solution is defined by $T(x,t) = T(x,t+P_0)$ for all x. In our simulations we require

$$\frac{1}{\text{total length}} \int {\rm d}x \left| T(x,t) - T(x,t+P_0) \right| < 10^{-6}. \tag{23}$$

Once the steady state is reached, the COP of the overall system shown in Fig. 5(a) is given by

$$\mathrm{COP}_{\mathrm{Pel}} = \frac{\bar{J}_0^-}{\bar{J}_n^+ - \bar{J}_0^-} \tag{24}$$

where $\bar{J}$ is the steady-state cycle-averaged heat flux

$$\bar{J} = \frac{1}{P_0}\int_0^{P_0} \mathrm{d}t\, J(t) \tag{25}$$

Multiplying $\bar{J}$ by the cross section gives the total cooling power.

B. Fixing model parameters and control variables

In all the subsequent simulations, we assume each MCM unit (blue rectangles) in Fig. 5(a) is of 0.1 cm thickness. The small value is chosen to reduce the entropy created by thermal conduction. This value is actually thinner than the Peltier module, but is completely plausible. More discussion on the thickness is given in Section V D. Once the MCM/Peltier configuration is fixed, there are two control degrees of freedom: the field applied to each MCM unit and the current applied to Peltier module. For the applied field, we consider the following two scenarios:

- (H1) The fields applied to all MCM units are according to $H_n(t)$ in Eqs. (20). In other words, we apply a time-varying but spatially uniform magnetic field to the entire MCM/Peltier configuration. This spatial-temporal field sequence is denoted as (H1).
- (H2) The fields applied to odd MCM units are according to $H_n(t)$ in Eqs. (20); those applied to even MCM units $\overline{H}_n(t)$. Note that in our labeling convention, the first MCM (MCM 1) is adjacent to the cold environment so that during the first half of the cycling period MCM 1 is at zero-field, low-temperature phase. This spatial-temporal field sequence is denoted as (H2). The main difference to (H1) is that the magnetic field of (H2) is not spatially uniform, which can be created by the "teeth" structure of the field source.

In all the following simulations we take P_0 of Eqs. (20) to be 1 sec, which is the shortest period allowed by the estimated relaxation time [see Section II B]. Note that according to Eqs. (20), each spatial point experiences one field value in the first half of the cycling period and the other value in the second half for both field sequences (H1) and (H2).

The current applied to each Peltier module will be specified explicitly by two vectors $\mathbf{I}_1$ and $\mathbf{I}_2$: the former for $t \in (0, P_0/2)$ whereas the latter for $t \in (P_0/2, P_0)$. We consider the applied currents of the following forms:

$$(\mathrm{H1}) \Rightarrow \begin{cases} \mathbf{I}_1 = [I_0^{(1)}, I_1^{(1)}, I_2^{(1)}, \cdots] \\ \mathbf{I}_2 = [I_0^{(2)}, I_1^{(2)}, I_2^{(2)}, \cdots] \end{cases}, \tag{26a}$$

$$(\mathrm{H2}) \Rightarrow \begin{cases} \mathbf{I}_1 = [I_0^{(1)}, I_b, I_2^{(1)}, I_b, \cdots] \\ \mathbf{I}_2 = [I_b, I_1^{(2)}, I_b, I_3^{(2)}, \cdots] \end{cases}. \tag{26b}$$

Note that the Peltier modules are labeled from 0 as indicated by the subscript. In (26b) the I_b, explicitly given in Eq. (9), is the current that results in a zero heat flux from the cold side of the Peltier module; it depends on the instantaneous temperatures on both sides of the Peltier device and is thus time-dependent. The applied currents of Eq. (26b) under (H2) are motivated by the cascade magnetocaloric device as discussed in Chapter 6 of Ref. [4] and Ref. [18], where the Peltier modules are used as thermal diodes during certain time in the cooling cycle. The basic strategy to determine the currents in Eqs. (26) is to remove more heat from the cold environment when the leftmost MCM is experiencing the low magnetic field and colder (low-field) whereas to eject more heat to the hot environment when the rightmost MCM is experiencing the high magnetic field and hotter. Practically, we shall scan the parameters in some restricted space. One general remark is emphasized. In the cascade arrangement, Peltier module is the only component that can provide heat flow against that generated by the environment. Therefore in any case, the applied current, if not zero, should *always* generate the convective heat flow (i.e., those from motions of charge carriers) opposite to that caused by environments.

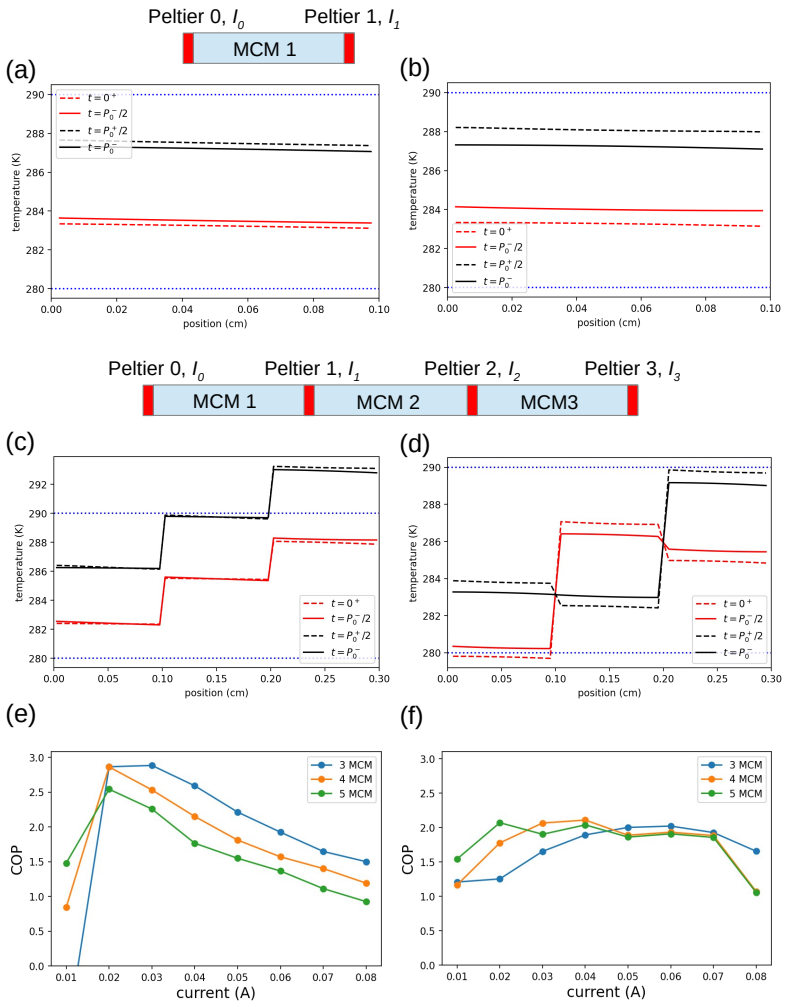

FIG. 6: MCM temperature as a function of space and time for configurations shown in Fig. 5(a). The schematic arrangement of 1 MCM unit [for (a), (b)] and 3 MCM units [for (c), (d)] are respectively given in the top and middle of the figure. Two blue dotted horizontal lines indicate two environment temperatures at 280 K and 290 K. (a) 1 MCM units with (H1) and $\mathbf{I}_1 = \mathbf{I}_2$ = (0.05, 0.05). (b) 1 MCM units with (H2) and $\mathbf{I}_1$ = (0.06, I_b), $\mathbf{I}_2$ = (I_b, 0.06). (c) 3 MCM units with (H1) and $\mathbf{I}_1$ = (0.04, 0.04, 0.04, 0.008), $\mathbf{I}_2$ = (0.03, 0.025, 0.025, 0.025). (d) 3 MCM units with (H2) and $\mathbf{I}_1$ = (0.03, I_b, 0.03, I_b), $\mathbf{I}_2$ = (I_b, 0.03, I_b, 0.04). The COP's for (a), (b), (c), (d) are respectively 3.18, 3.00, 3.98, 2.56. COP as a function of current defined in Eq. (27): (e) (H1) sequence; (f) (H2) sequence. $P_0 = 1$ is used in all calculations.

C. Simple configurations: 1 MCM and 3 MCM

Let us begin with the simplest configuration that contains only one MCM unit and three Peltier modules. After extensive parameter scans, two selected results using Eq. (26a) and Eq. (26b) are shown in Fig. 6(a) and (b), where the steady-state temperature distributions at four time instants, $t = 0^+$, $P_0^{\pm}/2$, and P_0^-, are plotted. Between $t = 0^-$ to 0^+, the field is removed from MCM and MCM is at its lowest temperature. From $t = 0^+$ to $P_0^-/2$, MCM is absorbing more heat from the cold environment than ejecting heat to the hot environment so its temperature is increasing. Between $t = P_0^-/2$ to $P_0^+/2$, the field is applied to MCM and MCM is at its highest temperature. From $P_0^+/2$ to $t = P^-$, MCM is ejecting more heat to the hot environment than absorbing heat from the cold environment so its temperature is decreasing.

At any instants except $t = NP_0$, $(N + 1/2)P_0$ (N being an integer), the temperature profile within each MCM appears flat with a small negative gradient. This feature is general (for both (H1), (H2) sequences and for multiple MCM units) and can be understood as follows. Once the applied field is fixed, thermal conduction is the only mechanism that accounts for the heat flow within an MCM. Since the heat flux J is controlled by the boundary values and $J = -\kappa_{\rm Gd}\frac{{\rm d}T}{{\rm d}x}$, the small $\left|\frac{{\rm d}T}{{\rm d}x}\right|$ (corresponding to the flat distribution) is a consequence of large $\kappa_{\rm Gd}$ and small J.

For cooling to take place, J is positive imposing a negative $\frac{\mathrm{d}T}{\mathrm{d}x}$.

With only one MCM unit, we do not find the applied currents leading to a COP that exceeds the maximum COP from a single Peltier module. When stacking more MCM units together, the COP could be enhanced. After random searches, the best results using 3 MCM units with (H1) and (H2) are given respectively in Fig. 6(c) and (d). The applied currents are provided in the caption. With 3 MCM units, the resulting COP shown in Fig. 6(c) is 3.98, larger than both maximum values given in Fig. 3(a) and (b). However we do not find an apparent trend that could guide the control process, so we proceed to scan parameter values in restricted space.

D. Parameter scan in restricted space

The searching parameter space grows linearly upon increasing the number of MCM units. To investigate the cooling performance involving more MCM's, we consider the following restricted one-dimensional subspace:

$$(\mathrm{H1})_{\mathrm{res}} \Rightarrow \mathbf{I}_1 = \mathbf{I}_2 = I \tag{27a}$$

$$(\mathrm{H2})_{\mathrm{res}} \Rightarrow \begin{cases} \mathbf{I}_1 = [I, I_b, I, I_b, \cdots], \\ \mathbf{I}_2 = [I_b, I, I_b, I, \cdots] \end{cases} . \tag{27b}$$

In the restricted space defined in (27), a constant current is applied to all Peltier modules for (H1) sequence whereas the current alternates between a constant and I_b for (H2) sequence. The resulting COP's using 3, 4, 5 MCM units are given in Fig. 6(e) and (f). It appears that generally COP's using Eq. (26a) is larger than (at least comparable to) those using Eq. (26b), but the overall performance in either sequence does not exceed that of a single Peltier module in the restricted space. We also try some random search but do not find any significant enhancement of COP [e.g., Fig. 6(c)].

E. Comparison to literature and summarizing statement

We end this section by comparing our setup to that by Monfared [18] where the cascade arrangement is investigated. First, the thickness of the Peltier module used in Ref. [18] is not thin. Because of its small thermal conductance, the passive "thick" Peltier module acts as a thermal diode; the current is applied to generate the heat flow. In contrast, for thin Peltier modules considered here, the thermal conductance cannot be neglected and the current of I_b [determined from Eq. (9)] is needed to block the conductive heat flow. It is interesting to notice that the role of applied current is somehow reversed in the thin and thick Peltier module; but they are all well described by the 3-parameter model described in Section II B. Second, Ref. [18] only investigates the scenario close to (H2) sequence, i.e., at any instant about half of Peltier modules act as thermal diodes. We relax this constraint and find the (H1) scenario, where none of Peltier modules completely block the heat flux at any time, is generally a better choice. Nonetheless, both studies agree that the overall performance using cascade arrangement is far worse than that using the conventional AMR setup.

As a brief summary, our numerical investigations suggest that the combination of magnetic cooling and Peltier modules could improve COP up to 10 or 20 % compared to that using a single Peltier module (given fixed environment temperatures). This enhancement does not justify the efforts to incorporate the magnetic cooling. The bottleneck is that the whole configuration can only exchange heat with environments via the Peltier modules, where increasing the heat flux is accompanied with Ohm loss that limits the COP. The qualitative result is consistent with the finding reported in Ref. [18]. We conclude that some other heat exchange channels have to be included and in Section V we shall reinsert the working fluid to further enhance the COP.

V. DIRECT CONTACT BETWEEN MCM AND ENVIRONMENTS

Up to this point, the configurations under consideration can only exchange heat with environments via the Peltier modules, and the resulting COP's are not significantly larger than that using a single Peltier module given fixed environment temperatures. Now we consider the configurations where MCM units at two ends exchange heat directly with two environments. In this setup, the requirement of Peltier modules becomes even lower as the heat exchange with environments is provided by other mechanisms.

A. Heat transfer between MCM and environment

We will consider the MCM's at two ends that directly exchange heat with the environments, as shown in Fig. 5(b). In this case, the environment also acts as heat source applied to MCM:

$$q_{\rm env}(x,t) = \underbrace{\frac{A_{\rm HT}}{V} h_{\rm HT}}_{\equiv h_{\rm eff}} \big[T_{\rm env} - T(x,t)\big], \tag{28}$$

where $x \in$ end MCM and $T_{\rm env} = T_{\rm cold}$ or $T_{\rm hot}$. $h_{\rm HT}$ is the heat transfer coefficient between the MCM and the environment; $\frac{A_{\rm HT}}{V}$ is ratio between heat-transfer area and the total volume. We consider two end MCM's exchanging heat with the flowing water, whose thermal conductivity is about $\kappa_{\rm water} \approx 0.006$ W/(cm·K). The heat transfer coefficient between MCM's and water is estimated using Nusselt correlation

$$h_{\rm HT} = {\rm Nu} \times \frac{\kappa_{\rm water}}{d_h}, \tag{29}$$

where Nu is the Nusselt number and d_h is the hydraulic diameter. As an estimation, we take $d_h = 0.2$ cm and Nu $= 7$ [30] that gives $h_{\rm HT} = 0.21$ W/cm^2 K; we further take $\frac{A_{\rm HT}}{V} \sim 8$ cm^{-1} to get $h_{\rm eff} \approx 1.7$ W/cm^3. This value will be used in the subsequent calculations. With n MCM units and $n-1$ Peltier modules as shown in Fig. 5(b), the cycle-average cooling power, heat rejection power, and the overall COP are respectively given by

$$J_{\rm L,env} = \frac{1}{P_0} \int_{\rm MCM\ 1} {\rm d}x \int_0^{P_0} {\rm d}t\, q_{\rm env}(x,t), \tag{30a}$$

$$J_{\rm R,env} = \frac{1}{P_0} \int_{\rm MCM\ n} {\rm d}x \int_0^{P_0} {\rm d}t\, q_{\rm env}(x,t), \tag{30b}$$

$${\rm COP}_{\rm env} = \frac{J_{\rm L,env}}{J_{\rm R,env} - J_{\rm L,env}}. \tag{30c}$$

We note that the $h_{\rm eff}$ value is just an order-of-amplitude estimation. In this setup, we need to consider some special treatment on the end MCM units, such as porous structure, to enhance the heat exchange to the environments.

B. Restricted control protocol

The cooling system involves several MCM units. To simplify the control protocol, we restrict the applied currents to Eqs. (27). Fig. 7 gives the selected temperature distribution as a function of time for (H1) and (H2) field that lead to large COP's. Results using 4 MCM units are shown in Fig. 7(a) and (b). For applied currents given in the caption of Fig. 7, the overall COP is about 9.3, about 2.6 times larger than the COP's given in Fig. 6(b). Results using 5 MCM units are shown in Fig. 7(c) and (d). With Eq. (27a) [Fig. 7(c)], the constant current of 0.025A gives a COP of 9.58, about 2.7 times larger than the COP's given in Fig. 6(b). With Eq. (27b) [Fig. 7(d)] in the restricted parameter space, we do not find the applied currents that give a large COP. More details for configurations in Fig. 7 are provide in Table II.

configuration info.	$J_{\rm L,env}$ (W/cm^2)	$J_{\rm R,env}$ (W/cm^2)	${\rm COP}_{\rm env}$	$I_{\rm ave}$
Fig. 7(a): (H1), 4 MCM	0.082008	0.090918	9.28	0.028
Fig. 7(b): (H2), 4 MCM	0.100267	0.110919	9.41	0.0315
Fig. 7(c): (H1), 5 MCM	0.087713	0.096863	9.58	0.025
Fig. 7(d): (H2), 5 MCM	0.137095	0.200174	2.17	0.0355

TABLE II: Detailed results of Fig. 7. The applied currents are given in Fig. 7; heat fluxes and COP are defined in Eq. (30). $J_{\rm L}$ corresponds to the (specific) cooling power. $I_{\rm ave}$ is the time-averaged current over a cycle.

The main reason leading to the sharp COP difference between Fig. 7(c) and (d) is the applied current. According to our analysis, the Ohm loss of Peltier module, which has I^2 dependence, is the main source of heat generation and the key factor that limits COP. As seen in the last column of Table II, the averaged current of Fig. 7(d) is about 42% larger than that of Fig. 7(c); In contrast the averaged current of Fig. 7(b) is only about 12.5% larger than that of Fig. 7(a). Larger current generally leads to larger cooling power; this is also seen in $J_{\rm L,env}$ values in Table II. We explicitly point out that in the setup considered here, the entire cooling device actually ejects heat to the cold environment over one half of the cycling period, but it absorbs more heat from $T_{\rm cold}$ over the other half of the period. The same statement holds applied to the heat ejected to $T_{\rm hot}$.

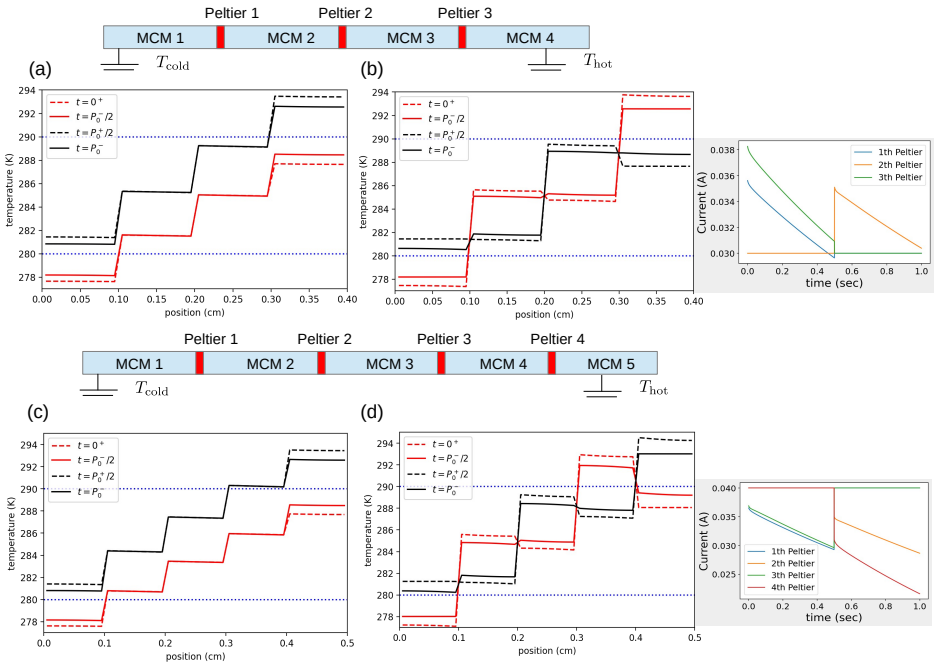

FIG. 7: MCM temperature as a function of space and time for configurations shown in Fig. 5(b). The schematic arrangement of 4 MCM unit [for (a), (b)] and 5 MCM units [for (c), (d)] are respectively given in the top and middle of the figure. Two blue dotted horizontal lines indicate two environment temperatures at 280 K and 290 K. (a) 4 MCM units with (H1) and $\mathbf{I}_1 = \mathbf{I}_2$ = (0.028,0.028, 0.028). (b) 4 MCM units with (H2) and $\mathbf{I}_1$ = (0.03, I_b, 0.03), $\mathbf{I}_2$ = (I_b, 0.03, I_b). (c) 5 MCM units with (H1) and $\mathbf{I}_1 = \mathbf{I}_2$ = (0.025, 0.025, 0.025, 0.025). (d) 5 MCM units with (H2) and $\mathbf{I}_1$ = (I_b, 0.04, I_b, 0.04), $\mathbf{I}_2$ = (0.04, I_b, 0.04, I_b). The COP's for (a), (b), (c), (d) are respectively 9.20, 9.41, 9.58, 2.17; those of (a), (b), (c) are about 3 times larger than the maximum COP's given in Fig. 3(a) and (b). The right panels of (b), (d) show the time-dependent applied current to each Peltier module.

C. (H1) field sequence and constant Peltier currents

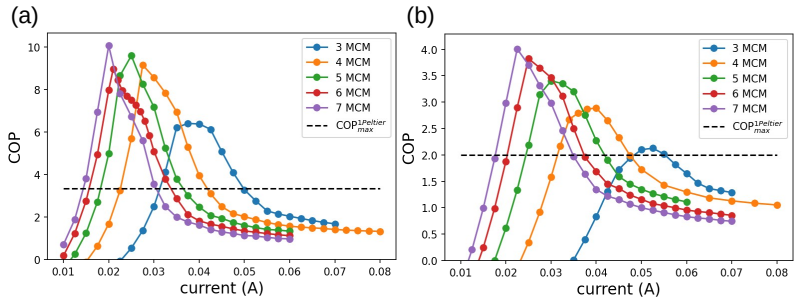

FIG. 8: COP as a function of the current applied to the Peltier module. (a) ($T_{\rm cold}, T_{\rm hot}$)=(280 K, 290 K) for 3-7 MCM units. (b) 5 MCM units and ($T_{\rm cold}, T_{\rm hot}$)=(275 K, 290 K) for 3-7 MCM units. Upon increasing the number of MCM units, the current corresponding to maximum COP reduces, meaning the cooling power also decreases. The dotted horizontal line indicates the $\mathrm{COP}_{\rm max}$ from a single Peltier module.

Our numerical analysis suggests that (H1) sequence performs at least comparable to (H2) sequence. Moreover when the MCM unit is thin, (H1) sequence that requires spatially uniform magnetic field is easier to realize. We thus systematically examine the scenario using the (H1) sequence with a constant current applied to *all* Peltier modules (i.e., all currents in Eq. (26a) are identical). The COP's of 3 MCM to 7 MCM units as a function of the applied current are given in Fig. 8(a). We clearly see that the maximum COP's are about three times larger than that using one single Peltier module. Upon increasing the number of MCM units, the maximum COP generally increases (expect that of 6 MCM units) but appears to saturate; the corresponding current and thus the cooling power decrease. To

confirm the generality of this behavior, we repeat the analysis for a larger temperature span of $T_{\rm cold} = 275$ K, $T_{\rm hot} = 290$ K. The results are shown in Fig. 8(b), and the similar conclusion is reached.

D. General remarks

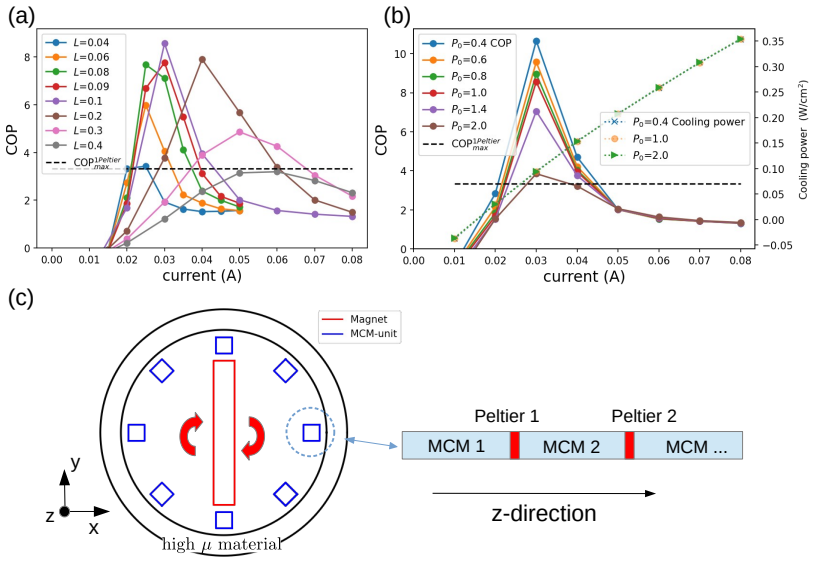

FIG. 9: COP as a function of the current applied to the Peltier module using 4 MCM units, (H1) sequence, and $(T_{\rm cold}, T_{\rm hot})$=(280 K, 290 K). (a) P_0=1s, and MCM thickness is from 0.04 cm to 0.4 cm. An optimal thickness around 0.1 cm is seen for this set of parameters. (b) MCM thickness is 0.1 cm, P_0=0.4s to 2.0s. Reducing the cycling period enhances the maximum COP without noticeably affecting the cooling power. Caveat: within our approximation, the relaxation time of Peltier module imposes a lower bound of period. (c) One potential structure to realize the overall magnetic cooling device for (H1) sequence. The spatially uniform, time-varying field can be generated by a rotating magnet, enclosed by a high-μ material. The designed MCM/Peltier module units are placed in the gap and do not move. The actual size of each MCM/Peltier module unit (right of (c)) could be around 1cm^2×4cm, depending on the number of stacked MCM; and sizes of other components are scaled accordingly. Two working fluids (not shown) connected directly to two environments are in contact with MCM at two ends.

We end this section by a few general remarks. The first one is about the field sequence. In a sense, (H1) sequence is based on the heat regeneration whereas (H2) on the cascading mechanism; both mechanisms aim to accumulate the modest temperature span built from one single magnetization/demagnetization process (about 4-5 K) to reach a meaningfully large temperature difference across the entire device. Using (H1) sequence, the Peltier modules act like the working fluid in the standard AMR, as they provide the convective channels to force the heat flux from the cold to the hot side. In fact, the temperature distributions shown in Fig. 7(a), (c) can be viewed as the zigzag approximation of those obtained in Fig.5 of Ref. [24]. Using (H2) sequence where a spatially alternating magnetic field is needed, Peltier modules serve as thermal diodes that block the heat exchange between certain pair of adjacent MCM units. Our simulations favor the AMR mechanism: (H1) sequence is not only easier to implement but also yields a comparable or larger COP. We stress that in the cascade arrangement, Peltier module is the only component that can generate heat flow against the environments. Since applying current has to come with Joule heating, to maximize the cooling performance the current applied to each Peltier module should always generate the convective heat flow (motion of charge carriers) opposite to that caused by environment.

The second one is about the thickness of MCM unit. Our simulations show that devices of thinner MCM units lead to larger COP's; this is true for both (H1) and (H2) field sequence. We can understand the thickness dependence from two aspects. First, the heat flux within a MCM unit is caused solely by heat conduction which generates entropy, and a thinner MCM generates less entropy. Second, by regarding the Peltier modules as the working fluid, thinner MCM units correspond to a larger contact area and the MCM and thus a more effective heat transfer. In the limit where MCM is negligibly thin, the COP is governed by the limit of Peltier modules. Therefore an optimal thickness is expected. An example using (H1) sequence is given in Fig. 9(a), where COPs for MCM thickness between 0.04cm to 0.4cm are shown. The optimal thickness occurs around 0.1 cm is clearly seen for the parameters given in the caption.

The third remark is about the cycling period. One of the motivations to use Peltier modules as thermal diodes is to reduce the cycling period and thus increase the cooling power [4, 15]. With cascade arrangement, our simulations show that given the same applied currents, reducing the period can increase the COP without noticeably affecting cooling power. Illustrative results are provided in Fig. 9(b), where we vary the period P_0 from 0.4s to 2.0s. We emphasize that the approximations used in our simulations limits the shortest period to be the relaxation time of the Peltier module. This degree of freedom needs more investigations [17]. The shortest period of 0.4s used in Fig. 9(b) corresponds roughly to the relaxation time of Si-based Peltier module reported in Ref. [25].

From Section III to V, by introducing more components to the cooling device we gradually lessen the burden of Peltier modules. In the end, a direct heat exchange between end MCM units and environments is needed to robustly enhance the COP (compared to that using a single Peltier module). We notice that the COP's considered in this work are still generally smaller than those using the conventional setup that allows the working fluid to exchange heat with *all* MCM's in the cooling device [4, 24]. The main reason is that that the Joule heating of Peltier module is larger than the viscosity loss of the working fluid. However, the fact that the working fluid does not enter the most of MCM units greatly simplifies the water pumping and valve systems, and we regard it as the practical advantage of integrating Peltier modules in the magnetic cooling device. Also, using MCM of Curie temperature specific to some target temperature range becomes easier in the cascade arrangement.

Finally, a potential realization is illustrated in Fig. 9(c). The spatially uniform, time-varying field is generated by a rotating magnet, enclosed by a high-μ material to confine the flux and thus enhance the field strength. The designed MCM/Peltier module units are placed in the gap and do not move. Two working fluids connected directly to two environments are in contact with MCM at two ends (fluids not shown). We think the large field has limited effects on Peltier modules. As the carrier motion inside the Peltier module is almost confined in one dimensional direction [see Fig. 2(a)] and does not form a closed loop, the induced voltage caused by the time-varying magnetic field is expected to be small [18]. Also, the field induced spin splitting is less than 10^{-3} eV (estimated from electron magnetic moment), much smaller than the bandgap (of order eV) and is not expected to be important.

VI. CONCLUSION AND FUTURE DIRECTION

In this work, we systematically consider the magnetic cooling device that uses Peltier modules to control the heat flux. We focus on the cascade arrangement where Peltier modules and MCM units are alternate in space: the MCM temperatures are controlled by the applied field; the heat flow between adjacent MCM's are controlled by the applied current. We adopt a 3-parameter model for Peltier modules and examine its validity by fitting to existing commercial products. When placing a Peltier module between MCM units, its effect can be approximated by a current-dependent discontinuity in heat flux. Doing so greatly simplifies the numerics as the thermal behavior, notably the transient response, within the Peltier module is neglected. With the developed formulation, we perform extensive parameter scans and show that to have a robust COP enhancement, the MCM units have to directly exchange heat with the environments. The practical advantage of integrating Peltier modules in the magnetic cooling device is to simplify the fluid pumping and valve design.

There are topics which worth further investigations. First, the transient behavior with the Peltier module is neglected, which is essential when the cycling period is short. One could explicitly include the Peltier module in the discretization, or consider other Peltier materials having shorter relaxation time. Second, our simulations use the field of 2T due mainly to its convenient experimental availability. With some interpolation scheme of experimental data, one could also describe the continuous field change and maybe treat the applied field as a control degree of freedom. For example, for a fixed number of MCM units, the best field strength may depend on the environment temperatures. Finally, one could explore more complicated applied currents to further enhance COP. However, since the cooling performance is very non-linear as a function of applied currents and steady-state simulations are time-consuming, it may be more practical to confine the search space within some (relatively) easily implementable schemes.

Acknowledgement

The author thanks William Vetterling and Chih-Kuan Tung (North Carolina A&T State University) for very helpful discussions and for carefully reading the manuscript. Insightful suggestions from anonymous reviewers are sincerely appreciated.

Appendix A: Estimation of Peltier parameters

Here we show how the Peltier parameters R, K, $\mathcal{S}$ are estimated from the product Spec sheet. The Specs of two selected models are shown in Table III: R is directly measured; ($\Delta T_{\max}$, $T_{\rm hot}$, $T_{\rm cold}$) and $V_{\Delta T_{\max}}$ are sufficient to estimate K and $\mathcal{S}$; $I_{\Delta T_{\max}}$ and $J_{\max}$ will be used as self-consistency checks. Once R, K, $\mathcal{S}$ are determined, $\mathcal{S}/A$, R/A and K/A with A the cross section of the module.

module #	dimension (cm)	R (Ω)	($\Delta T_{\max}$, $T_{\rm hot}$, $T_{\rm cold}$)	$V_{\Delta T_{\max}}$	$I_{\Delta T_{\max}}$	$J_{\max}$
CP081030-M	1×1×0.3	9.85	(68, 300, 232)	8.8 V	0.8 A	3.7 W
CP200543636	5.4×3.6×0.36	0.33	(70, 300, 230)	8.5 V	20 A	96 W

TABLE III: Specs of two Peltier modules taken from from "https://www.cuidevices.com/catalog/thermal-management/peltier-modules" (the product is chosen randomly; reference herein does not constitute or imply its endorsement). Temperature is in Kelvin. In the last column $J_{\max}$ is measured at $T = 300$K.

R, K, $\mathcal{S}$ of CP081030-M are determined as follows: Eq. (5a) with $T_{\rm cold} = 232$ K gives $\mathcal{S} = 0.0293$ V/K; Eq. (4) with $\Delta T_{\max} = 68$ K and $T_{\rm cold} = 232$ K gives $\mathcal{Z} = 0.0025$ K^{-1}; $\mathcal{Z} = \frac{\mathcal{S}^2}{RK}$ gives $K = 0.035$ W/K. Dividing R, K, $\mathcal{S}$ by the cross section of 1 cm^2 leads to the values provided in Table I. Using the estimated R, K, $\mathcal{S}$ we do the following self-consistency checks: Eq. (5b) gives $I_{\Delta T_{\max}} \approx 0.7$, about 12% smaller than the measured 0.8 A; Eq. (5b) gives $J_{\max}(T = 300\text{K}) \approx 3.9$ W, about 5% higher than the measured 3.7 W.

Similarly for CP200543636: Eq. (5a) with $T_{\rm cold} = 230$ K gives $\mathcal{S} = 0.0283$ V/K; Eq. (4) with $\Delta T_{\max} = 70$ K and $T_{\rm cold} = 230$ K gives $\mathcal{Z} = 0.0026465$ K^{-1}; $\mathcal{Z} = \frac{\mathcal{S}^2}{RK}$ gives $K = 0.919$ W/K. Dividing R, K, $\mathcal{S}$ by the cross section of 19.44 cm^2 leads to the values provided in Table I. Using the estimated R, K, $\mathcal{S}$: Eq. (5b) gives $I_{\Delta T_{\max}} \approx 19.74$, about 1.2% smaller than the measured 20 A; Eq. (5b) gives $J_{\max}(T = 300\text{K}) \approx 109.47$ W, about 14% higher than the measured 96 W. We have gone through this procedure for tens of Peltier modules, and found that the typical errors in the self-consistency check are $\lesssim 5\%$.

[1] G. V. Brown, Journal of Applied Physics **47** (1976).
[2] V. K. Pecharsky and K. A. Gschneidner, Jr., Phys. Rev. Lett. **78**, 4494 (1997), URL https://link.aps.org/doi/10.1103/PhysRevLett.78.4494.
[3] V. K. Pecharsky and K. A. Gschneidner, Jr., Journal of Magnetism and Magnetic Materials **167**, L179 (1997), ISSN 0304-8853, URL https://www.sciencedirect.com/science/article/pii/S0304885396007597.
[4] A. Kitanovski, J. Tušek, U. Tomc, U. Plaznik, M. Ožbolt, and A. Poredoš, *Magnetocaloric Energy Conversion: From Theory to Applications* (Springer International Publishing, 2015).
[5] W. A. Steyert, Journal of Applied Physics **49**, 1216 (1978).
[6] K. Gschneidner and V. Pecharsky, International Journal of Refrigeration **31**, 945 (2008), ISSN 0140-7007, URL https://www.sciencedirect.com/science/article/pii/S0140700708000236.
[7] S. Tassou, J. Lewis, Y. Ge, A. Hadawey, and I. Chaer, Applied Thermal Engineering **30**, 263 (2010), ISSN 1359-4311.
[8] U. Tomc, J. Tušek, A. Kitanovski, and A. Poredoš, Applied Thermal Engineering **58**, 1 (2013), ISSN 1359-4311, URL https://www.sciencedirect.com/science/article/pii/S1359431113002706.
[9] U. Tomc, J. Tušek, A. Kitanovski, and A. Poredoš, International Journal of Refrigeration **37**, 185 (2014), ISSN 0140-7007.
[10] D. Silva, A. Pereira, J. Ventura, J. Araújo, and J. Oliveira, Journal of Magnetism and Magnetic Materials **533**, 167979 (2021), ISSN 0304-8853, URL https://www.sciencedirect.com/science/article/pii/S0304885321002559.
[11] D. E. Rowe, *Thermoelectrics Handbook: Macro to Nano (1st ed.)* (CRC Press, 2006).
[12] G. Nolas, J. Sharp, and J. Goldsmid, *Thermoelectrics: Basic Principles and New Materials Developments* (Springer, 2001).
[13] G. Wehmeyer, T. Yabuki, C. Monachon, J. Wu, and C. Dames, Applied Physics Reviews **4**, 041304 (2017).
[14] K. Klinar and A. Kitanovski, Renewable and Sustainable Energy Reviews **118**, 109571 (2020).
[15] A. Kitanovski and P. W. Egolf, International Journal of Refrigeration **33**, 449 (2010), ISSN 0140-7007, URL https://www.sciencedirect.com/science/article/pii/S0140700709002527.
[16] W. de Vries and T. H. van der Meer, Applied Thermal Engineering **111**, 377 (2017).
[17] H. Huang, J. Shen, Z. Li, K. Li, P. Hai, W. Zheng, R. Huang, and W. Dai, Applied Thermal Engineering **217**, 119056 (2022), ISSN 1359-4311, URL https://www.sciencedirect.com/science/article/pii/S1359431122009887.
[18] B. Monfared, International Journal of Refrigeration **74**, 324 (2017).
[19] T. F. Petersen, K. Engelbrecht, C. R. H. Bahl, B. Elmegaard, N. Pryds, and A. Smith, Journal of Physics D: Applied Physics **41**, 105002 (2008), URL https://doi.org/10.1088/0022-3727/41/10/105002.
[20] Z. Zheng, H. Yu, X. Zhong, D. Zeng, and Z. Liu, International Journal of Refrigeration **32**, 78 (2009), ISSN 0140-7007, URL https://www.sciencedirect.com/science/article/pii/S0140700708001217.
[21] J. Tušek, A. Kitanovski, and A. Poredoš, International Journal of Refrigeration **36**, 1456 (2013).

[22] S. Y. Dan'kov, A. M. Tishin, V. K. Pecharsky, and K. A. Gschneidner, Phys. Rev. B **57**, 3478 (1998), URL https://link.aps.org/doi/10.1103/PhysRevB.57.3478.
[23] T. Hashimoto, T. Numasawa, M. Shino, and T. Okada, Cryogenics **21**, 647 (1981), ISSN 0011-2275, URL http://www.sciencedirect.com/science/article/pii/001122758190254X.
[24] J. Tušek, A. Kitanovski, I. Prebil, and A. Poredoš, International Journal of Refrigeration **34**, 1507 (2011).
[25] Y. Furubayashi, T. Tanehira, A. Yamamoto, K. Yonemori, S. Miyoshi, and S.-I. Kuroki, ECS Transactions **80**, 77 (2017).
[26] H. S. Kim, K. Kikuchi, T. Itoh, T. Iida, and M. Taya, Materials Science and Engineering: B **185**, 45 (2014), ISSN 0921-5107, URL https://www.sciencedirect.com/science/article/pii/S0921510714000361.
[27] T. Arisaka, M. Otsuka, and Y. Hasegawa, Review of Scientific Instruments **90**, 046104 (2019).
[28] J. B. Pendry and A. MacKinnon, Phys. Rev. Lett. **69**, 2772 (1992), URL https://link.aps.org/doi/10.1103/PhysRevLett.69.2772.
[29] C. Lin, Journal of Applied Physics **125**, 093904 (2019).
[30] A. Bejan and A. D. Kraus, *Heat Transfer Handbook* (Wiley-Interscience, 2003).